A&A 427, 637–649 (2004)
DOI: 10.1051/0004-6361:20040348

Astronomy & Astrophysics

Improved fundamental parameters for the low-mass pre-main sequence eclipsing system RX J0529.4+0041⋆,⋆⋆

E. Covino[1], A. Frasca[2], J. M. Alcalá[1], R. Paladino[3], and M. F. Sterzik[4]

[1] INAF - Osservatorio Astronomico di Capodimonte, via Moiariello 16, 80131 Napoli, Italy
e-mail: covino@na.astro.it
[2] INAF - Osservatorio Astrofisico di Catania, via S. Sofia, 78, Città Universitaria, 95123 Catania, Italy
[3] INAF - Osservatorio Astronomico di Cagliari, Loc. Poggio dei Pini, Strada 54, 09012 Capoterra, Cagliari, Italy
[4] European Southern Observatory, Casilla 190001, Santiago 19, Chile

Received 27 February 2004 / Accepted 21 July 2004

Abstract. We report new photometric observations and a new determination of the fundamental stellar parameters for the low-mass pre-main sequence eclipsing system RX J0529.4+0041A based on high-precision, near-IR (*JHK*) differential photometry obtained using adaptive optics at the ESO-La Silla 3.6 m telescope, and $UBV(RI)_C$ CCD photometry performed with the OIG camera at TNG. The new photometric data, in combination with already published photoelectric photometry and solution of the radial velocity curve, yield a more precise determination of the absolute dimensions and masses as well as of other basic physical properties of the components.

Key words. stars: pre-main sequence – stars: binaries: eclipsing – stars: binaries: spectroscopic – stars: fundamental parameters – stars: individual: RX J0529.4+0041 – stars: binaries: close

1. Introduction

The location of young stars on the H-R diagram is commonly used to infer their masses and ages from the comparison with computed pre-main sequence (PMS) evolutionary tracks and isochrones. In spite of the considerable amount of theoretical work devoted in the last two decades to the development of PMS evolutionary models, the currently available evolutionary tracks from different authors yield somewhat different predictions, in terms of mass and age, especially in the solar and lower mass stars regime (see for example Baraffe et al. 2002). This is mainly because the models still suffer from severe uncertainties both in the input physics and in the treatment of the complex phenomena accompanying the early evolutionary phases of a star (for example, the burning of light elements and the treatment of convection during the Hayashi phase), which are determinant factors for the calculation of the observable properties of a star (e.g. effective temperature and luminosity). These uncertainties heavily affect the estimations of stellar masses and ages, and have strong consequences for the derivation of the initial mass function (IMF), and for reconstructing the star formation history of a given region, in particular in the low- and very low-mass regimes. Thus, the comparison of fundamental stellar parameters derived directly from observations with the predictions from evolutionary model calculations provides a crucial test in order to discriminate among different models as well as to provide a "mass calibration" for the available sets of PMS tracks.

Unfortunately, from the observational side, the lack of direct information on fundamental stellar parameters for low-mass PMS stars of different masses and ages still prevents such a test from being realised and does not yet allow one to constrain the models. The situation is still unsatisfactory even for the low main sequence, since eclipsing systems with low-mass components are extremely rare, mainly because of observational limitations. The very few determinations of stellar parameters available to date indicate that the current models tend to underestimate the radius (by up to 20%) and to overestimate the effective temperature (by about 150 K), whereas ages might be overestimated by up to a factor 10 (Torres & Ribas 2002).

The study of binary systems, through the measurement of the dynamical mass of two gravitationally bound components orbiting each other, represents the only way to test theoretical evolutionary models and to provide the absolute mass calibration for PMS tracks in the H-R diagram, as well as a relative age calibration for the theoretical isochrones. Indeed, the component stars in relatively short-period systems most likely originated from a common star formation event, and they should hence be coeval. Thus, they are expected to

⋆ Based on observations carried out at ESO, La Silla, Chile, (ESO prop. 66.C-0469, 68.C-658) and at TNG, La Palma, Spain (TAC 4_06).
⋆⋆ Full Table 1 and Appendix A are only available in electronic form at http://www.edpsciences.org

"trace" an *observational isochrone*. Among all kinds of binary stars, spectroscopic and eclipsing systems offer the best means to test theoretical evolutionary tracks, as they allow, through the combined analysis of radial velocities and photometric curves, the determination of all stellar fundamental parameters of the components in one step (Andersen 1991). However, until now, this possibility has been hampered by the extreme rarity of eclipsing systems and the difficulty of finding them among PMS stars. A more extended, systematic search would require relatively large amounts of dedicated time on small/intermediate size (1 m class) telescopes (unfortunately a dying species), in order to intensively monitor large numbers of objects in nearby star formation regions.

While many spectroscopic binaries with main-sequence components, in the field and in open clusters, have been studied and their orbital elements have been derived, so that the circularization time is determined for the population of binaries belonging to young clusters and for the two older binary populations of M 67 and of the Galactic Halo, for the PMS binaries Mathieu (1994) counted only 25 systems with known orbital elements. These numbers have been increasing in recent years thanks to the discovery of many weak-T Tauri stars (WTTS) as optical counterparts of X-ray sources (mainly in the ROSAT All-Sky Survey) in the nearby star-forming regions. The preliminary results of on-going spectroscopic monitoring surveys on these stars (Alcalà et al. 2002; Covino et al. 2001; Melo et al. 2001) have revealed that many of them are indeed spectroscopic binaries. Among these we discovered the first eclipsing binary composed of two low-mass stars, RX J0529.4+0041 (Covino et al. 2000).

In this paper we determine anew the fundamental stellar parameters for the two low-mass components of the PMS eclipsing binary system RX J0529.4+0041A, based on near-infrared (*JHK*) and $UBV(RI)_{\rm C}$ CCD photometry.

Although unfavorable weather conditions at TNG prevented us from achieving a good coverage of the eclipse phases in the optical bands, these data proved to be quite useful to constrain the physical parameters of the binary components (e.g. $T_{\rm eff}$ and radii) as they, in combination with the infrared photometry, allowed us a "multiwavelength" approach to the light-curve solution.

2. Observations and data reduction

2.1. Near-infrared adaptive optics photometry

Sequences of high-angular resolution images of RX J0529.4+0041 were obtained in the near-infrared *J*, *H* and *K* bands using the ADaptive Optics Near Infrared System (ADONIS), mounted at the ESO 3.6 m telescope at La Silla Observatory (Chile), equipped with the System for High Angular Resolution Pictures (SHARP) II near infrared (NIR) imaging camera with a NICMOS III array. A plate scale of 0.050 arcsec/pixel, yielding a camera field-of-view of $12\farcs8 \times 12\farcs8$, was used (see Beuzit et al. 1997; and Hofmann et al. 1995, for more details).

The orbital period, of nearly exactly 3 days, and the short duration of the eclipses (less than 6 h), determined by previous photoelectric photometry in the *B* and *V* bands (Covino et al. 2000), posed quite strong constraints on the observation scheduling. The observations were thus planned on two separate nights, December 6th 2000 and January 12th 2001, in which, based on the ephemerides available to us (Covino et al. 2001), the primary and secondary minima were expected to occur in the middle of the night, under the most favorable observability conditions for La Silla. The observations were successfully carried out, and both the primary and secondary eclipses could be entirely monitored. Additional observations using the same instrumental set-up were ensured on three consecutive nights in 2001, from December 6th to 8th, with the aim to check the stability of the light-curve with time as well as to gather at least a partial coverage at different out-of-eclipse phases. This was in fact the last opportunity to gather additional data using the same instrument, as ADONIS was decommissioned after ESO Period 69.

The main advantage of using an AO system is that it provides diffraction limited resolution in the core of the Point Spread Function (PSF) (i.e. $0\farcs15$ in the *K*-band). This allowed us to fully resolve, in each of the *J*, *H*, and *K* bands, the two visual components of RX J0529.4+0041, at about $1\farcs3$ separation. Since our targets are relatively bright they were used as reference stars for wavefront sensing. Overheads for the AO system and NIR camera setting were of the order of a few minutes. In order not to lose time resolution, we chose: 1) not to optimize the AO system performance when switching to the next filter and the result of this choice was a lower resolution in the *J* and *H* bands; 2) to spend the minimum time in adjusting the individual integration time, although the PSF peak intensity may vary by more than 10% between consecutive frames.

The integration times were set to 30 s in *J* and 20 s in *H* and *K* filters for all exposures of the target. Near-IR photometric standard stars taken from the ARNICA Catalogue (Hunt et al. 1998) were observed at the beginning and end of the night, under similar sky transparency conditions, to obtain absolute *JHK* photometry. As measured by the La Silla Differential Image Motion Monitor (DIMM), the atmospheric seeing during our run varied with time, ranging from $0\farcs8$ to $1\farcs2$.

Unfortunately, the measurements of time turned out not to be as accurate as we would have expected. Time was not registered in the FITS header of each ADONIS frame, but could only be inferred from the UT "hour" and "minute" of the computer clock which was recorded, without any rounding-off of the seconds, in the corresponding file-name. This implied a possible inaccuracy of up to 1 min on the time-axis which, at the phases where the light variation is faster, may affect the data by an amount comparable to the photometric uncertainty.

For the reduction of the ADONIS images we used our own procedures based on the ESO/*Eclipse* (Vers. 3.4) data reduction routines (Devillard 1997), running under Unix. The background emission was computed for every pixel as a median value of the stack of frames. For each exposure the following reduction steps were applied: i) subtraction of background sky emission; ii) division by flat-field; iii) correction for bad pixels by applying a bad-pixel map; and iv) "shift-and-add" method to yield the final images.

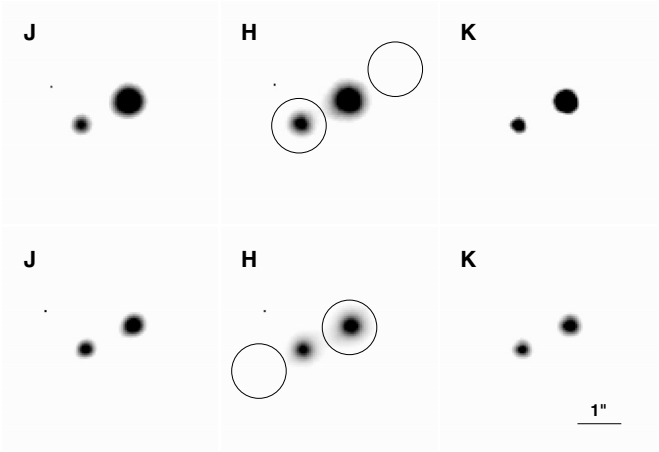

Fig. 1. ADONIS images of the eclipsing PMS binary RX J0529.4+0041A (upper-right star) and its companion in the J, H, and K bands. North is down, East to the left. The three upper images show the eclipsing system at maximum brightness, whereas the lower ones are close to the primary minimum. In the upper and lower middle frames the apertures used for measuring each component and the corresponding sky are also drawn.

2.1.1. Differential *JHK* photometry

As expected, the new, extremely sharp, ADONIS images of RX J0529.4+0041 allowed us to fully resolve the eclipsing system from its visual companion and to separately measure each of them by aperture photometry (see Fig. 1), The photometric measurement of the stars in the ADONIS field was performed by using a semi-authomatic IDL procedure, specifically written by us for this task, which calls the IDL APER routine adapted from DAOPHOT. Moreover, taking advantage of the fact that the two visual components, thanks to their relatively large separation ($1\farcs35 \pm 0\farcs01$), appeared fully resolved on all of the ADONIS images, we could also use the companion as a comparison star to measure the relative light variations of the eclipsing system in the J, H and K bands. Indeed, the differential photometry proved to reduce significantly the scatter in the resulting light-curves with respect to absolute measurements, but, of course, we wanted first to probe the stability of the companion on different nights. Absolute photometry was thus used to check the visual companion for possible varability, indicating that this star was fairly stable (within about 1%) on the different nights of the run. This indication received further confirmation after the excellent match obtained in the differential light-curve between the two secondary minima observed by us almost one year apart.

In order to properly take into account the mutual light contamination of the two stars the sky background was measured at diametrically opposite positions with respect to each component, as shown in the central panels of Fig. 1.

In order to derive the best quality light-curves from our data for the subsequent analysis, differential photometry in the J, H, and K bands of RX J0529.4+0041A with respect to the visual companion used as a comparison star was obtained. Estimated errors of the differential measurements are of the order of 0.005 mag or lower.

Table 1. *JHK* differential photometry of the eclipsing component RXJ 0529.4+0041 A with respect to component B, with running Heliocentric Julian Day (−2, 400, 000). The corresponding orbital phase is computed using the new ephemeris given in Sect. 4.1 (only in electronic form).

HJD	Phase	ΔJ
+51 886.55859	0.95086	−0.980
+51.....	.....	.....

HJD	Phase	ΔH
+51 886.55859	0.95086	−0.925
+51.....	.....	.....

HJD	Phase	ΔK
+51 886.56250	0.95215	−0.915
+51.....	.....	.....

In Table 1 we report the differential J, H, and K magnitudes of RX J0529.4+0041A with respect to the visual companion versus the Heliocentric Julian Day.

2.1.2. Absolute *JHK* photometry

Taking advantage of the prolonged observation of the target field during large part of the night, and spanning a wide range of air mass, atmospheric extinction coefficients in the J, H and K bands were determined, for each night, from the measurements of the visual companion, RX J0529.4+0041B, instead of adopting the (somewhat lower) mean values for La Silla. Zero Points to convert the instrumental magnitudes to absolute photometry were determined from the *JHK* standard stars observed at the beginning, middle, and end of the night. Our Zero Point determinations, obtained by measuring the standard stars through an aperture of 60 pixels radius, were found to be in excellent agreement with the values provided under the ESO-La Silla Web site[1].

Mean *JHK* magnitudes for the visual components of RX J0529.4+0041 are reported in Table 2. The values for component A correspond to maximum brightness (out-of-eclipse phases).

2.2. $UBV(RI)_C$ CCD-photometry

CCD photometry in the $UBV(RI)_C$ bands (R and I in the Cousins photometric system) was obtained on the two nights, 2000 November 19th and 2001 January 5th, using the Optical Imager of Galileo (OIG) at the Galileo National Telescope (TNG) at La Palma (Canarias islands, Spain), operated in service mode. Although in changeable weather conditions, and affected by interruptions due to technical reasons, some useful data could be obtained on November 19th, which cover the rise from the primary minimum, while on January 5th the

[1] http://www.ls.eso.org/lasilla/Telescopes/360cat/adonis/html/sharp_calib.html

Table 2. Absolute photometry for the visual components, A (eclipsing binary) and B (companion), of RXJ 0529.4+0041. All magnitudes involving component A refer to out-of-eclipse phases, thus providing the mean maximum-light level.

Comp	U	B	V	R	I	J	H	K
A+B	14.00 ± 0.05	13.30 ± 0.05	12.35 ± 0.04	11.70 ± 0.04	11.15 ± 0.03	–	–	–
A	14.19 ±0.07	13.54 ± 0.06	12.61 ± 0.05	11.99 ± 0.05	11.46 ± 0.05	10.73 ± 0.02	10.17 ± 0.02	10.03 ± 0.02
B	15.99 ± 0.10	15.04 ± 0.08	14.01 ± 0.07	13.29 ± 0.06	12.66 ± 0.06	11.76 ± 0.02	11.15 ± 0.02	11.01 ± 0.02

observation of the secondary minimum was completely hampered by bad weather conditions. Data reduction was performed using IRAF[2].

Absolute $UBV(RI)_C$ mean magnitudes (in the Johnson-Cousins photometric system) of RX J0529.4+0041 at maximum light are reported in Table 2, and are derived from already available calibrated *UBV* photoelectric photometry obtained, during out-of-eclipse phases, at Catania Observatory (Covino et al. 2000) under photometric sky conditions, combined with OIG $UBV(RI)_C$ data.

During most of the OIG observations the two visual components were not resolved, however, on some of the images obtained at maximum light the seeing was below 1.0 arcsec, allowing us to resolve the two components and measure their magnitude difference in the $UBV(RI)_C$ bands, in an analogous way as for *JHK*. The photometry of the two optically resolved A and B components is reported in Table 2, and the measurements of component A correspond to maximum light. We could hence also obtain the differential *UBVRI* magnitudes of component A with respect to component B, from their combined magnitudes, using the photometry reported in Table 2 for the resolved, A and B components, and the procedure described in the Appendix to correct for the third-light.

3. Complementary information

Our study makes use of distinct but complementary sets of information. These involve the results of the analysis of radial velocity curve reported in Table 3, light-curve, and spectral energy distribution (SED). The combined results provide a complete description of the gross physical properties of the system and a precise measurement of its distance. We exploit our already published results (radial velocity curves and spectral type determinations) from high-resolution spectroscopy (Covino et al. 2001) as well as new absolute multi-band photometry. Indeed the solution of the spectroscopic orbits yields the minimum absolute size of the system and individual minimum masses, which depend on the inclination of the orbital plane. On the other hand, the light-curve solution constrains the relative sizes and temperature ratio of the components, while the absolute value of the effective temperature for at least one of the components need to be determined by means of some calibration external to the light-curves.

[2] IRAF is distributed by the National Optical Astronomy Observatory, which is operated by the Association of the Universities for Research in Astronomy, Inc., under contract with the National Science Foundation.

Table 3. Orbital elements and stellar parameters of RXJ 0529.4+0041A from the spectroscopic orbits. The Epoch T_0 refers to the time of maximum velocity of the primary.

Quantity	Value(s)	
	Primary (1)	Secondary (2)
P_{orb} (days)	3.03772 ± 0.00001	
T_0 (HJD–2 400 000)[a]	51336.1194 ± 0.0013	
e	0.	
γ (km s^{-1})	+18.99 ± 0.14	
$q = M_2/M_1$	0.7305 ± 0.0025	
$K_{1,2}$ (km s^{-1})	80.58 ± 0.15	110.31 ± 0.30
$a_{1,2} \sin i$ (10^9 m)	3.3661 ± 0.0067	4.6080 ± 0.0130
$M_{1,2} \sin^3 i$ ($M_\odot$)	1.2652 ± 0.0080	0.9242 ± 0.0045

3.1. Radial velocity data

The solution of the radial velocity curves reported by Covino et al. (2001) provided a precise determination of the mass ratio and individual masses (apart from the factor $\sin^3 i$) of the eclipsing components. The latter, combined with the orbital inclination obtained from the light-curve solution, convert into absolute masses.

3.2. Spectral types and colours of the components

The spectral types of the components, yielding information on the effective temperatures of the stars, provide very important constraints on the input parameters for the analysis of the light curves of eclipsing binary systems. In particular it is critical, in order to achieve a reliable evaluation of the effective temperature of the Secondary from the light-curve analysis, to rely on a good determination of the spectral type of the Primary component so that its effective temperature can be adopted as a fixed input parameter. To this purpose, we adopt the revised spectral types derived by Covino et al. (2001) through a matching of the binary spectrum with that of a synthetic binary. Details on the application of the spectral subtraction technique and on the radial and rotational velocities determination are given in Covino et al. (2000, 2001).

The spectral type of K1 $V \pm 1$ spectral subclass restricts the allowed T_{eff} for the Primary component to the range 5000–5300 K. The value of 5025 K, derived from the de Jager & Nieuwenhuijzen (1987) calibration, was originally adopted for the B and V light-curve solution in Covino et al. (2000).

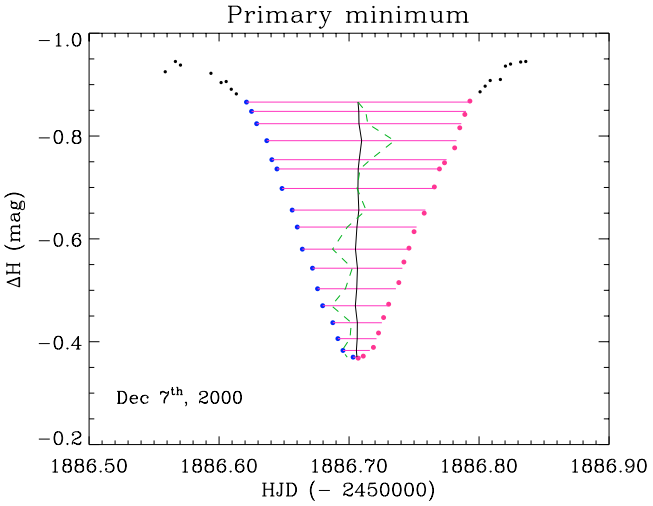

Fig. 2. Example of the bisector method used to determine the time of a minimum. The vertical solid line represents the bisector for primary eclipse data in the H band, whereas the dashed line shows the bisector on a ten times expanded scale.

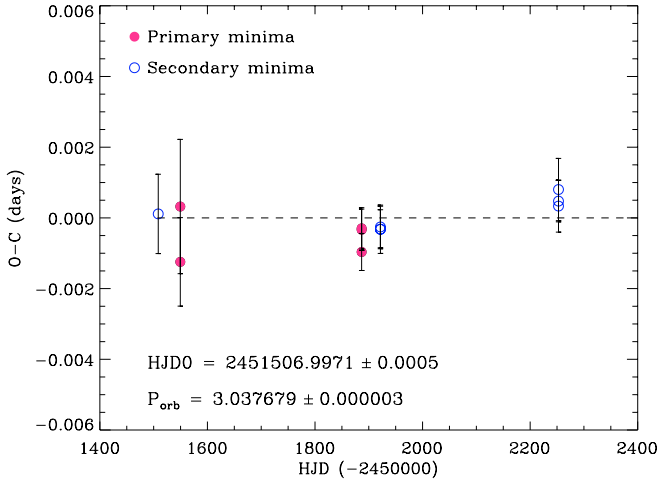

Fig. 3. Observed minus calculated times of minima for the eclipsing system RX J0529.4+0041A. Primary and secondary minima are represented with filled and open circles respectively. The orbital period appears to be constant within the errors.

A spectral classification of K7–M 0 for the secondary component was derived from spectral synthesis of composite binary spectra in Covino et al. (2001).

Additional constraints on the effective temperature of the primary component can be obtained from the observed colours at the secondary minimum, when the light contribution from the secondary, although not totally eclipsed, becaoms drastically reduced (by as much as nearly 90%). Thus, the colour information can actually help to set a lower limit to the effective temperature of the primary. The best suited appear to be the $B-V$ and $V-K$ colours, in combination with colour-to-effective temperature calibrations. Using the $B-V$ colour has the advantage that B and V data are simultaneous and the contributions from the secondary and tertiary components are relatively less important. The third-light corrected magnitudes $V = 12.61$ and $B = 13.54$ (from Table 2), become, at the secondary minimum, 12.77 and 13.67, respectively, giving $B-V = 0.90$. This, adopting a value of $E(B-V) = 0.10$ mag, for the distance of 325 pc, yields $B-V = 0.80$, which would correspond to $T_{\rm eff} = 5234$, adopting the Alonso et al. (1996) calibration, or to $T_{\rm eff} = 5282$, using the one from Flower (1996). A $(V-K)_0$ value of 2.05 at the secondary minimum is obtained from the measured K magnitude at phase 0.5, and the combined V magnitude corrected for the third light at the same phase, adopting $A_V = 0.325$ and $A_K = 0.040$ for the interstellar extinction. This yields $T_{\rm eff} = 5050$ K, using Alonso et al. calibration.

4. Light-curve analysis

4.1. New ephemeris

The orbital period has been re-determined from the times of the observed photometric minima.

In order to reduce the uncertainties on the mid-eclipse epochs due to the measurement errors, the time of each minimum was obtained applying the bisector method to the well observed minima (including both descending and rising branches), as illustrated in Fig. 2, where the jitter in the eclipse bisector induced by the photometric noise is clearly visible. The standard deviation of the mid-eclipse epochs is in the range from about 50 to 150 s, depending on the data S/N and on the sampling rate. In Fig. 3 we plot the difference between the observed epochs of primary (filled circles) and secondary minima (open circles) and those obtained from the ephemeris of constant period which gives the best match to the data:

$$T_{\rm MinI}({\rm HJD}) = 2\,451\,506.9971(5) + 3.037679(3) \times E \qquad (1)$$

where the numbers in parentheses indicate the error on the last digit.

The O−C diagram reported in Fig. 3 shows that a constant period ephemeris is able to reproduce the observed epoch of minima within the errors, with all O−C residuals scattered around zero, although it might also contain a hint for an increasing period which needs additional data to be confirmed.

4.2. Light-curves solution method and model approximations

We used the differential photometry of compenent A relative to component B obtained in each band, following the usual approach to eclipsing binary light-curve modelling (see Wilson 1994, for a comprehensive review on the subject). The solution of the three near-infrared light-curves in the J, H, and K bands was performed using the program *Nightfall*, written by R. Wichmann[3], based on Roche geometry. The fit to the observed light-curves was obtained using the option of the program which evaluates the flux contribution of the two components in the observed bands by means of model atmospheres. Although the system is clearly well detached (as indicated by the sharpness of the eclipses), reflection and proximity effects were also considered using the algorithm described in Djurašević (1992).

[3] http://www.lsw.uni-heidelberg.de/~rwichman/Nightfall.html

The best-fit solution to the observed light-curves was found under the following assumptions and using the following program options:

- circular orbits, as inferred from the *RV* curves and confirmed by the phase difference of 0.5 between the primary and secondary minima;
- limb darkening approximated by a square root law. A square-root form was adopted as it seems to behave better than linear or quadratic ones. The values of the coefficients are chosen on the basis of the spectral type of each component and of the observed wavelengths (Van Hamme 1993);
- gravity darkening, caused by the nonsphericity of the stars in the Roche geometry, is modelled in the code by the adoption of a local effective temperature dependent on the local gravity. For convective stars (below 7000 K) a temperature-dependent gravity brightening exponent is used (Alencar 1997);
- the flux contribution of each component is obtained from a grid of synthetic low-resolution spectra for $\log g = 4.0$ and solar chemical composition, deriving from the detailed numerical computations of NextGen model atmospheres by Hauschildt et al. (1999a,b);
- for the calculation of the heating effect by mutual irradiation of the components, the bolometric albedo was fixed for both stars to the standard value of 0.50, typical of stars with convective envelopes (Rucinski 1969). Reflection effect is accounted for by a "detailed" treatment, through iteration over all pairs of surface elements $(\mathrm{d}S_1, \mathrm{d}S_2)$ and summing up, for each surface element $\mathrm{d}S_1$, the irradiation by all visible surface elements $\mathrm{d}S_2$ of the other star (Hendry & Mochnacki 1992);
- synchronous rotation of the components with the orbital motion. The limits of validity of this simplifying assumption can be checked a posteriori using the derived stellar radii and the measured projected rotational velocities for the two components (Covino et al. 2001).

The light-curve solution was performed by keeping as fixed input parameters the mass ratio $q = M_2/M_1 = 0.7305$, determined from the RV-curve solution, the orbital period refined from all the available times of minima, and the effective temperature of the Primary, and by leaving as free parameters the inclination of the orbit i, the radius of the primary component R_1, the effective temperature and radius of the secondary component, T_2, and R_2.

Actually, *Nightfall* uses as a measurement of the size of the stars the filling factor of each component, *RocheFill*, defined as the ratio between the polar radius of the star and the polar radius of its Roche lobe. Allowed values for *RocheFill* are in the range 0.001–1.3 (values above 1.0, indicate stars merging into a *common-envelope/overcontact* system). Initial values of the fit parameters were taken from the previous, combined radial-velocity and light-curve solution (Covino et al. 2001). Additionally, several trials were also performed running *Nightfall* with different starting values for the parameters to make realistic estimates of the uncertainties and to test the uniqueness of the solution.

While the depths of the eclipses in different bands constrain the ratio of the stellar temperatures, in order to establish the absolute temperature scale, the temperature of the primary component needs to be evaluated independently from color and/or spectral type informations. However, even with precise masses, the test of PMS tracks might be invalidated because of uncertainties on the effective temperatures of the two components. Thus, the light-curve solution was also performed adopting for the primary component extreme values for its plausible temperature range, compatible with its spectral type of K0–K1, and depending on different temperature scale calibrations, e.g. 4950–5300 K (Houdashelt et al. 2000; Cox 2000; Gray 1992; de Jager & Nieuwenhuijzen 1987). This test showed that the effect of varing the temperature of the primary component by ±100 K, produces a change in the resulting temperature of the secondary of nearly the same amount whereas it does not affect significantly the other parameters (e.g., the orbital inclination and the stellar radii). Therefore, the uncertainty on the temperature of the Secondary should not be significantly larger than that quoted for the Primary component.

In principle, only the analysis of several, fully covered light-curves in different photometric bands, obtained at various epochs, can help to average out both measurement errors and intrinsic variations (as due, for example, to changing distributions of spots) in order to achieve a reliable determination of the parameters. Therefore, with the aim to check the long-term stability of the light-curve, the observation of the secondary eclipse was repeated in a second epoch, about eleven months later. As seen from Fig. 6 these two secondary minima overlap perfectly when folded in phase with the ephemeris given in Eq. (1). Thus, although more observations would be obviously desired, we can suppose rather confidently that the light-curve was stable over the time span of our observations.

4.2.1. Solution of *JHK* light-curves

As the $UBV(RI)_C$ photometry of RX J0529.4 +0041A incorporates the light from the close visual companion, whereas the *JHK* bands does not, before any attempt to perform a simultaneous light-curve solution of the optical and near-IR data, the former data need to be corrected for the contribution from the third light.

The first light-curve solution was thus performed on the *JHK* data and, initially, also the presence of stellar spots on either of the eclipsing components was not considered. However, the computed light-curves are unable to provide a really satisfactory match to the observational data, as they cannot reproduce the variation of the out-of-eclipse level, suggesting the likely presence of large photospheric spots on at least one of these late-type components. In particular, the computed light-curves do not reproduce the exact depths of the eclipses because of the notably different out-of-eclipse levels around the primary and secondary minima, apparent in the J, H, and K as well as in the more complete B and V light-curves (Covino et al. 2000). Thus, in order to achieve a more reliable fit, the out-of-eclipse variation needs to be taken into account.

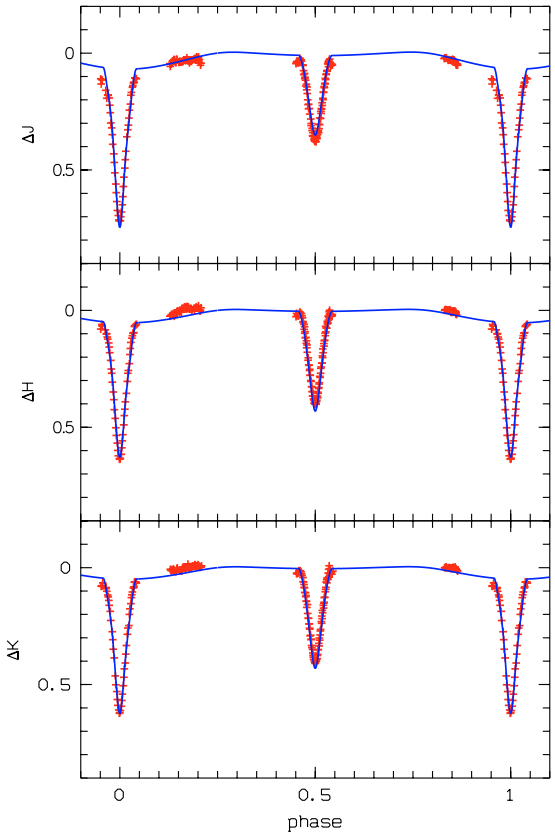

Fig. 4. *JHK* light-curve solution of RX J0529.4+0041A with 2 spots on the primary component, at 0°, −25°, and 180°, 42°, of 20° and 14° radius, respectively.

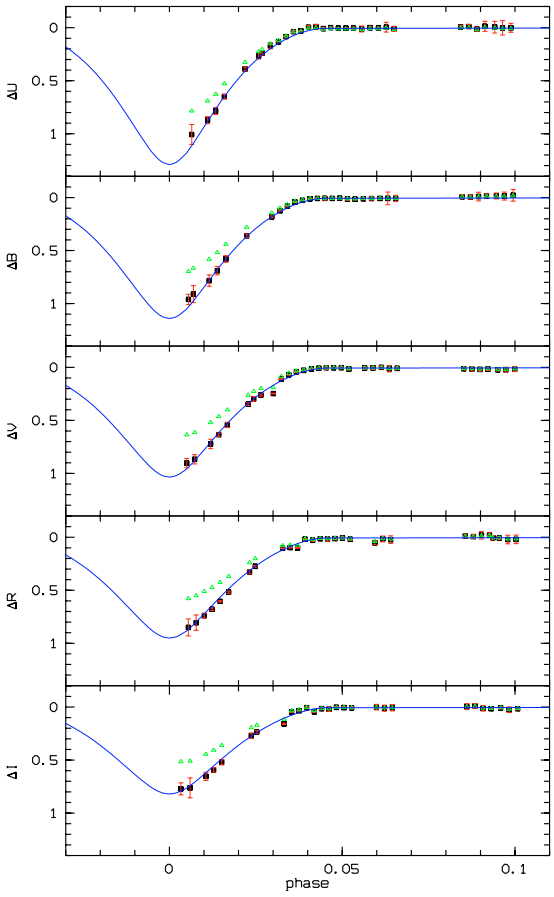

Fig. 5. Normalized *UBVRI* light-curves in proximity of the primary minimum as obtained from measurements on OIG images, inclusive of the "third light" (light triangles), and after correction for the "third-light" contribution (black squares), using the corresponding measurements for component B given in Table 2, as outlined in the Appendix. The corrected data match fairly well the synthetic light-curves (solid curves) calculated from solution of the *J*, *H*, and *K* bands only.

The presence of photospheric spots is to alter the out-of eclipse level, and hence the relative depth and the duration of the minima. Therefore, if not properly accounted for, this can cause systematic effects, in particular on relative temperature and radii of the components. However, as the information contained in the light-curve is insufficient to establish the exact location of spots on eather component, we explored this scenario by running several light-curves solutions with inclusion of up to two cool spots on the surface of each component. In order to achieve a satisfactory fit to the data, at least two, diametrically opposed spots on the hotter component are needed. The first solution obtained from *JHK* ignoring the presence of spots yielded a radius for the primary about 15% bigger than a solution in which stellar spots are included. Figure 4 shows the light-curve fit obtained with two circular spots located on the primary component: the first, at longitude 0° and latitude −25°, with 20° radius and temperature of 3120 K, the second, at longitude 180° and latidute 42°, with 14° radius and temperature 4370 K, respectively. The latitude, spot radius, and dimming factor (i.e., the ratio of the local temperatures with and without spot) of the spots were let as free parameters, whereas the latitude was kept fixed.

4.2.2. Simultaneous solution of *BV, JHK* light-curves

In order to exploit the full potential of the wide wavelength range (from optical to near-IR) covered by our data, we finally performed the simultaneous solution for the whole set of *B*, *V*, *J*, *H*, and *K* light-curves, after correcting the *B* and *V* data for the contribution from the third light. We obtained the differential *UBVRI* magnitudes corrected for the third-light, using the photometry reported in Table 2 for the resolved, A and B components, following the procedure described in the Appendix.

Figure 5 shows the comparison of the OIG data, before and after correction for the third-light, with the synthetic light-curves calculated from a solution of the *JHK* light-curves only. The net effect of the correction is to change the relative depths of the eclipses, as also clearly seen from the figure.

After this test, the correction for the third light was hence applied to all the other available optical data, using the direct measurents of component B in the corresponding bands, reported in Table 2.

Notice that we did not include the *U*, *R*, *I* light-curves in the final analysis because of the lack of photometric coverage. Also, due to lack of simultaneity of the optical and near-IR observations and to incomplete phase coverage of the *JHK* data,

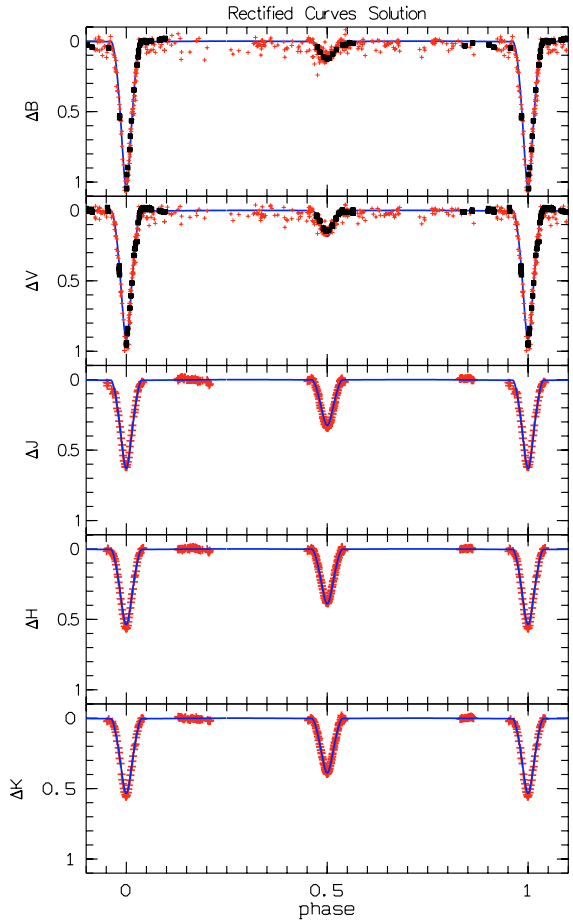

Fig. 6. Best-fit, simultaneous solution of the differential *B*, *V*, *J*, *H*, and *K* light-curves of RX J0529.4+0041A with respect to the visual companion, used as a comparison star. *B* and *V* differential magnitudes have been corrected for the third light contribution, following the method exposed in the Appendix. Light symbols represent the photoelectric data obtained at Serra La Nave (Covino et al. 2000), black dots indicate the CCD data from TNG.

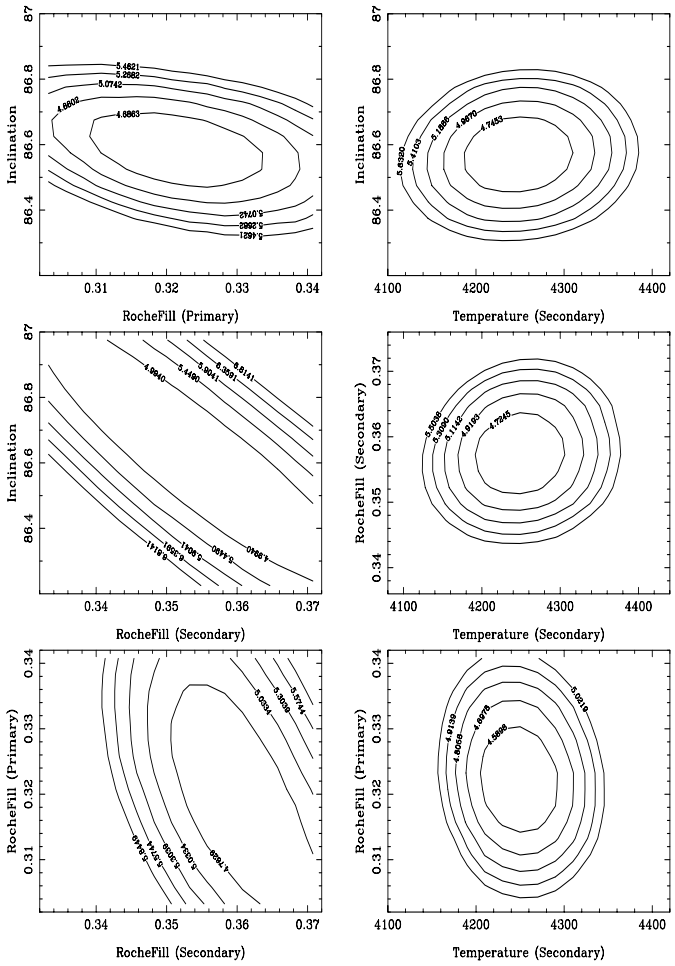

Fig. 7. χ-square maps for different pairs of light-curve parameters, adopting for the primary component the $T_{\rm eff}$ of 5200 K.

the only meaningful way to perfom a combined solution of the five bands simultaneously was to proceed with the rectification of the out-of eclipse level in the light-curves (Wilson 1994). This was achieved by removing from each light-curve the wave-like distortion ascribable to photospheric spots.

In this final analysis we also solved for the following light-curve parameters: the orbital inclination, the temperature of the secondary, and the radii of the two stars. The resulting stellar parameters are reported in Table 4, together with their corresponding formal mean standard errors. χ-square maps, produced with *Nightfall* for different pairs of parameters around the best-fit solution, are shown in Fig. 7. For comparison purposes, Table 4 also gives the corresponding results of the fit to the *JHK* light-curves with two spots on the primary component from Sect. 4.2.1. For same temperature of the Primary, the solution with spots yielded larger radii for both the primary and secondary component, 1.58 and 1.49 $R_{\odot}$, respectively, and an effective temperature of the Secondary about 120 K cooler.

Changing the temperature of the primary component from 5000 to 5300 K to account for uncertainties in its spectral type (±1 subclass) as well as to allow for possible systematic differences introduced by the adoption of a given temperature scale calibration, the temperature of the Secondary passes from nearly 4000 to about 4300 K, whereas the other free parameters remain practically unchanged (e.g. the orbital inclination varies from 86.37 to 86.53, and the radii of the primary and secondary components vary from 1.39 to 1.44 $R_{\odot}$ and, respectively, from 1.41 to 1.35 $R_{\odot}$). Thus, assuming those extreme values for the temperature of the Primary, the derived temperature for the Secondary also changes by nearly 300 K. Thus, the uncertainty on the temperature of the Secondary is essentially dominated by the uncertainty on the temperature of the Primary. The best among the best-fit solutions is found adopting an effective temperature for the Primary of 5200 K. This result turns out to be in line with the analysis of the spectral energy distribution reported in Sect. 5.

The final stellar physical parameters adopted from the light-curve analysis are listed in Table 5. The uncertainties quoted in this table were adopted not from the formal probable errors on the solution but rather performing additional trial solutions to account for the uncertainties on the adopted input parameters.

Several sets of starting parameters were tried in order to fully explore the parameter space around the best-fit solution. The scatter in the resulting parameters from numerous

Table 4. Best-fit parameters from model solutions of the *JHK* light-curves with 2 spots on the primary component and *BV*, *JHK* (rectified) light-curves, corresponding to an effective temperature of the Primary component of 5200 K. The quoted uncertainties are formal mean standard errors to the solution.

Parameter	Best-fit value	
(units)	2-spots	no-spots
i (deg)	87.0	86.53 ± 0.03
T_2 (K)	4100	4220 ± 50
$Rochefil_1$ [a]	0.36	0.33 ± 0.01
$Rochefil_2$ [a]	0.39	0.36 ± 0.02
Ω_1 [b]	8.03	8.73 ± 0.01
Ω_2 [b]	9.07	9.87 ± 0.01
χ^2	12.70	3.4873
$\sigma\,(B)$	–	0.0021
$\sigma\,(V)$	–	0.0019
$\sigma\,(J)$	0.0012	0.0011
$\sigma\,(H)$	0.0013	0.0007
$\sigma\,(K)$	0.0011	0.0006

Notes to table:
[a] Dimensionless, Roche-lobe filling factor, defined as $Rochefil_{1,2} = R_{\rm pole1,2}/R_{\rm lobe1,2}$.
[b] Dimensionless, Roche potential at stellar surface (see Djurašević 1992).

Table 5. Adopted stellar physical parameters for the eclipsing components of RXJ 0529.4+0041A.

Quantity	Value (1)	Value (2)
	Primary	Secondary
$M_{1,2}\,(M_\odot)$	1.27 ± 0.01	0.93 ± 0.01
$R_{1,2}\,(R_\odot)$	1.44 ± 0.05	1.35 ± 0.05
$T_{\rm eff1,2}\,(K)$	5200 ± 150	4220 ± 150
$\log g$ (cgs)	4.22 ± 0.02	4.14 ± 0.02
$L_{1,2}\,(L_\odot)$	1.37 ± 0.25	0.52 ± 0.15

additional solutions yields the estimated uncertainties that are generally several times larger than the internal statistical errors and we consider to be more realistic. For illustrative purposes, χ-square maps for different pairs of parameters around the best-fit solution are shown in Fig. 7.

Table 5 summarises the physical stellar parameters that we finally adopt for the components in the subsequent comparison with PMS evolutionary models.

5. Spectral energy distribution (SED) of the visual components and physical parameters for RX J0529.4+0041 B

We use the $UBV(RI)_{\rm C}JHK$ absolute photometry for the visual (A and B) components of RX J0529.4+0041, to derive the effective temperature and radius of component B adopting the same distance inferred for the eclipsing system and to verify the consistency of the results obtained for the latter from light-curve analysis.

5.1. Composite SED for RX J0529.4+0041 A

The spectral energy distribution (SED) of RX J0529.4+0041 A, reported in the upper panel of Fig. 8, was constructed from the dereddened, $UBV(RI)_{\rm C}JHK$ observed fluxes (black dots). These are compared with calculated fluxes (triangles) obtained from a combination of two synthetic Next-Generation spectra, corresponding to the physical parameters derived from the light-curve solution for each of the two eclipsing components. Also drawn in the figure are the individual and total synthetic spectra.

5.2. Physical parameters for component B

Based on spectroscopic evidences (presence of Lithium and common systemic radial velocity), there are good reasons to believe that RX J0529.4+0041 A and B do form a physically bound hierarchical triple system. Therefore it can be assumed to have the same distance from the Sun and the same age of RX J0529.4+0041 A.

Since RX J0529.4+0041 B is presumably single (spectroscopic data seem to rule out a possible SB nature), we can locate it in the HR diagram with fairly good accuracy exploiting the information gained from the study of the inner binary. The key parameter needed for the conversion from visual magnitude to luminosity is the distance of the system. Its value could be obtained in a very simple way with the "bolometric flux" method (see Gray 1992), which requires only the radii and effective temperatures of the eclipsing components A1 and A2 and the bolometric corrections. However, since we have data in several bands from near-UV to near-IR, we preferred to match the observed spectral energy distribution (SED) with synthetic spectra.

We evaluated the flux emitted in the optical and IR regions by the inner binary RX J0529.4+0041 A from the average, out-of-eclipse, $UBVR_{\rm C}I_{\rm C}JHK$ combined magnitudes (Table 2).

After standard correction for interstellar reddening (Savage & Mathis 1979, for A_R and A_I), adopting the value $E(B-V) = 0.10$, we obtained the $UBVR_{\rm C}I_{\rm C}JHK$ fluxes at Earth (in erg cm^{-2} s^{-1} Å^{-1}) for the central wavelength of each band (Lamla 1982).

These observed fluxes were compared with those obtained by integrating, into the proper pass-bands, the composite spectrum obtained by combining, with the proper weights, two synthetic low-resolution spectra matching the two eclipsing components of RX J0529.4+0041 A generated with the NextGen (Hauschildt et al. 1999a,b) photospheric models and available on the web[4].

The total flux at Earth $f_\lambda^{\rm tot}$ was obtained from the stellar surface fluxes of the individual synthetic spectra, $F_\lambda^{1,2}$ according to the relation

$$f_\lambda^{\rm tot} = F_\lambda^1 \frac{R_1^2}{d^2} + F_\lambda^2 \frac{R_2^2}{d^2}, \qquad (2)$$

where the radii $R_{1,2}$ are obtained from the light-curve solution and the distance has been let as a free parameter for the fit in

[4] http://dilbert.physast.uga.edu/~yeti/NG-spec.html

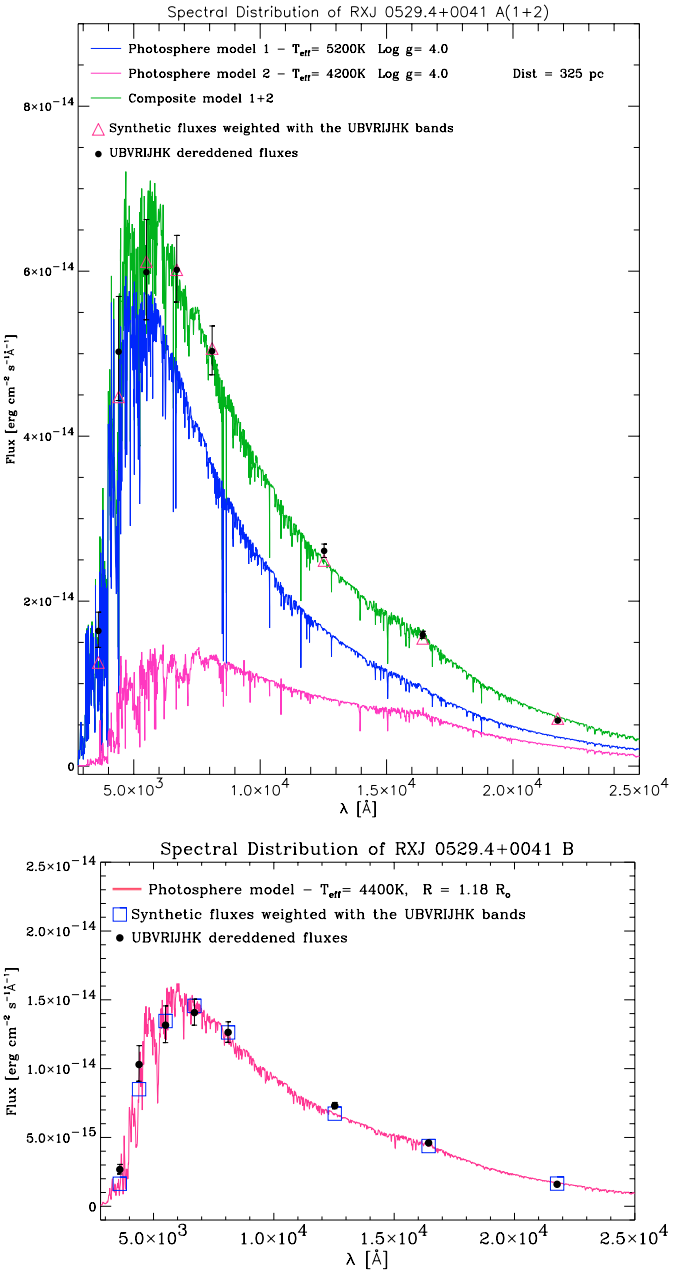

Fig. 8. *Upper panel*: spectral energy distribution (SED) of RX J0529.4+0041 A, as deduced from observed $UBV(RI)_{\rm C}JHK$ fluxes (dots), compared with calculated ones (triangles), obtained from a combination of two synthetic Next-Generation spectra with effective temperatures of 5200 K and 4200 K (continuous thin lines). *Lower panel*: comparison between observed (dots) and computed (squares) SED of RX J0529.4+0041 B, superimposed on the synthetic Next-Generation spectrum (thin continuous line) for $T_{\rm eff}$ = 4400 K.

which we have minimized the sum of residuals between observed and computed $UBV(RI)_{\rm C}JHK$ fluxes. We find a distance of 325 pc, with lower and upper limits, 310 and 340 pc, respectively, assuming the extreme values for radii and temperatures allowed from the light-curve fit. An idea of the accuracy of this procedure can be inferred by the dispersion of the distance values obtained from observed and calculated fluxes in the individual bands, for the derived values of radii and temperatures.

Table 6. Fundamental stellar properties for the components of RX J0529.4+0041A, NTT 045251+3016 (Steffen et al. 2001) and V1174 Ori (Stassun et al. 2004).

Quantity	RX J...A	NTT...	V1174 Ori
M_1 ($M_\odot$)	1.27 ± 0.01	1.45 ± 0.19	1.01 ± 0.01
M_2 ($M_\odot$)	0.93 ± 0.01	0.81 ± 0.09	0.73 ± 0.01
$\log T_{\rm eff,1}$	3.72 ± 0.01	3.64 ± 0.02	3.65 ± 0.01
$\log T_{\rm eff,2}$	3.63 ± 0.02	3.55 ± 0.02	3.56 ± 0.01
$\log L_1$ ($L_\odot$)	0.14 ± 0.08	−0.12 ± 0.05	−0.19 ± 0.05
$\log L_2$ ($L_\odot$)	−0.28 ± 0.15	−0.51 ± 0.09	−0.76 ± 0.06

The values span from 287 pc for the U band, to 309 pc for the B, 328 pc for the V, 325 pc for the R and I, 320 pc for the J and H, up to 331 pc for the K band.

In order to derive the effective temperature and luminosity of component B, we used a method similar to the one described previously, in which a single synthetic spectrum was used to reproduce the observed SED. We fixed the distance to the value found for the inner binary (325 pc) and let $T_{\rm eff}$ and $\log g$ of the model as well as the star radius to vary. The model with $T_{\rm eff}$ = 4400 K, $\log g$ = 4.0 and a star radius R = 1.2 $R_\odot$ gives the best match to the observed SED (see Fig. 8). The star radius we deduce for RX J0529.4+0041 B is in fairly good agreement with the value of 1.3 $R_\odot$ derived by means of the Barnes-Evans relation for late-type stars (Barnes et al. 1978) between the intrinsic $(V-R)$ colour index, the V apparent magnitude and the stellar angular diameter ϕ:

$$\log \phi = 0.4874 + 0.858(V-R) - 0.2V. \quad (3)$$

In Fig. 8 the observed distribution of $UBV(RI)_{\rm C}JHK$ fluxes at Earth (dots) is compared with the fluxes computed from the model (squares) as well as with the synthetic spectrum.

5.3. H-R diagramme

Finally, the masses, effective temperatures and luminosities for the eclipsing components are compared with the theoretical values inferred from evolutionary models, adopting various sets of PMS evolutionary tracks calculated by different authors.

Figure 9 shows the positions on the HR diagramme corresponding to the stellar parameters derived from the new light-curve solution reported in Table 5, compared with different sets of PMS evolutionary tracks and isochrones.

Additional mass determinations for low-mass PMS stars have become available in the literature. Therefore, on the HR diagramme of Fig. 9 we also report for comparison purposes the components of the astrometric-spectroscopic system NTT 045251+3016, with dynamical masses of about 1.4 and 0.8 $M_\odot$ respectively (Steffen et al. 2001), and those of the new eclipsing-spectroscopic binary V1174 Ori, of about 1.0 and 0.7 $M_\odot$ (Stassun et al. 2004). The fundamental parameters for these two systems and RX J0529.4+0041 A, are summarised in Table 6. The different positions of each pair of stars in the HR diagramme can be interpreted in terms of age differences for these systems, although metallicity might in principle

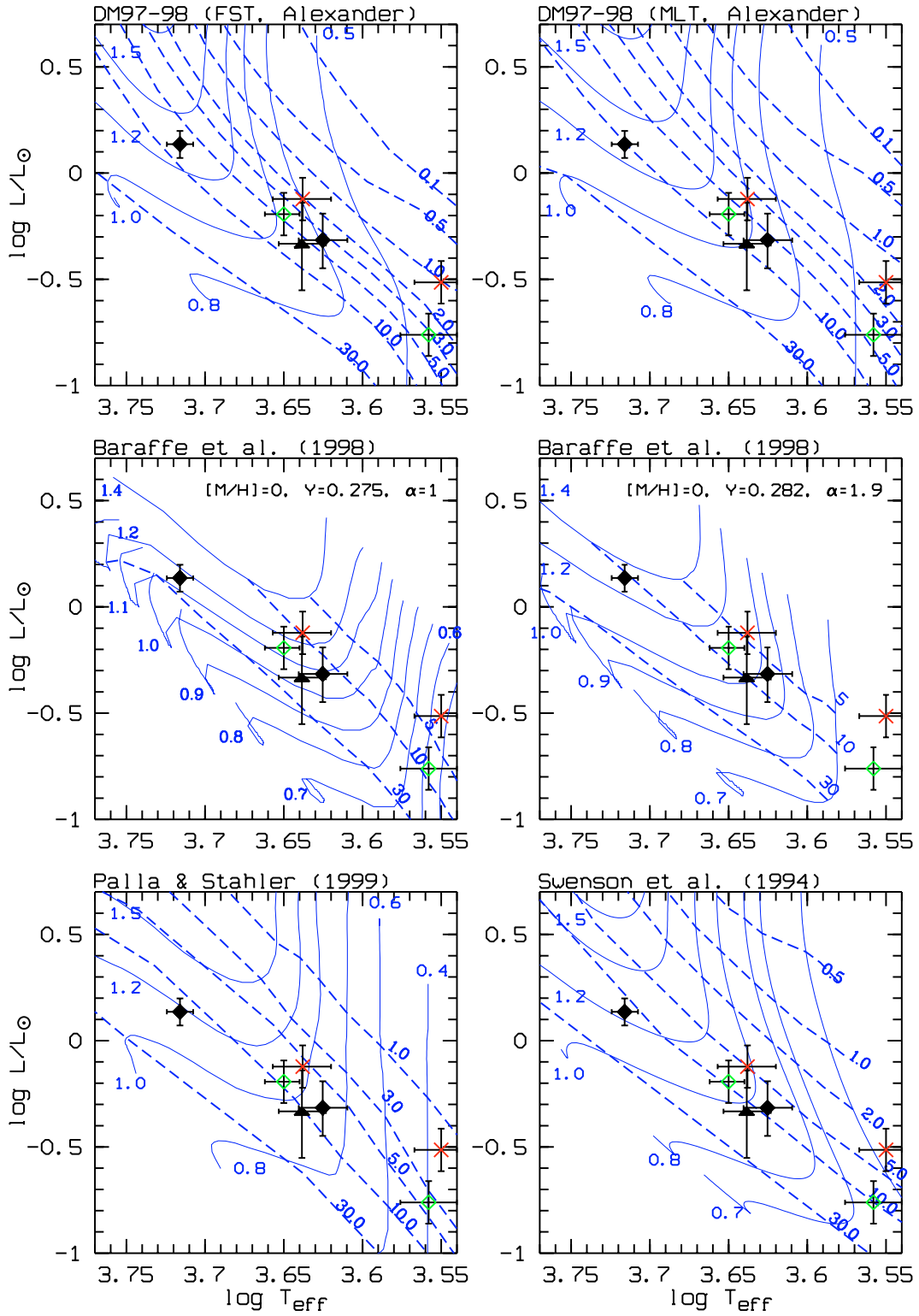

Fig. 9. Comparison on the HR diagramme of the positions of the eclipsing components of RX J0529.4+0041A (black diamonds) with different sets of PMS evolutionary tracks and isochrones from different authors. The position of the third component, RX J0529.4+0041B, is marked by the triangle. Tracks corresponding to different masses (solid lines) are labelled in solar units and isochrones (dashed lines) at different ages are marked in Myrs. Additionally, the positions of the components of the eclipsing system V1174 Ori (Stassun et al. 2004; small, open diamonds) and of the spectro-astrometric binary NTT 045251+3016 (Steffen et al. 2001; × symbols) are also shown.

also play a role. However, we notice that while for V1174 Ori, analogously to RX J0529.4+0041 A, the dynamical masses are accurate to about 1%, in the case of NTT 045251+3016 the accuracy appears somewhat lower, mainly due to the still relatively large uncertainty on the orbital inclination deriving from the not yet complete coverage of the astrometric orbit.

Indeed, the dynamical masses derived for the components of NTT 045251+3016 appear clearly inconsistent with their position on the HR diagramme as both the primary and secondary components are slightly cooler than the corresponding component of V1174 Ori, suggesting comparable (or slightly lower) masses.

With the present stellar parameter determinations, a better agreement between dynamical and theoretical masses is found for RX J0529.4+0041 A, and marginally also for V1174 Ori, in the case of the Swenson et al. tracks, and those from Baraffe et al. corresponding to a value of the mixing length parameter, $\alpha = l_{\rm mix}/H_{\rm P} = 1.9$. On the other hand, when compared to D'Antona & Mazzitelli's tracks, the Secondary of RX J0529.4+0041 A appears to be somewhat cooler for the FST tracks set, and better consistent to the MLT set of tracks. However, D'Antona et al. (2000) have shown that the purely thermal effect of a magnetic field can deeply modify the behavior of atmospheric convection, increasing the temperature gradients and lowering the effective temperature of the model. From the observational point of view, the results of the light-curve analysis also showed that the presence of spots represent a critical issue for the determination of stellar parameters, as they may affect the derived radii and alter the mean temperature of the components. Another key point to consider is that models for single, non-rotating stars might be inadequate to reproduce the properties of relatively fast-rotating stars.

Altough not helpful in the definition of absolute ages, PMS binary components at least provide a very good relative test for theoretical isochrones, as they are expected to be coeval. Remarkably, the components of the two eclipsing systems RX J0529.4+0041 A, and V1174 Ori, all lie very close to the same (10 Myr) isochrone of the Swenson et al.'s set. However, the slope of the *observed* isochrone appears to differ significantly from a theoretical one for all the other models except in the case of Baraffe et al.'s ($\alpha = 1.9$) models, which are marginally consistent with the observations.

Furthermore, using the results from Sect. 5.2, it is possible to locate the visual component, RX J0529.4+0041 B, on the H-R diagramme. Indeed, the high Li content in all of the three components and their common, systemic radial velocity, consistent with that of the Orion region, provide, altogether, strong independent support to the fact that the three of them are still in the PMS phase and most likely coeval.

6. Remarks and conclusions

The major trigger for the present work was the rather striking mismatch between the observed $T_{\rm eff}$ for the secondary component of RX J0529.4+0041 A (Covino et al. 2000, 2001) and the predictions by current models. Notoriously, theoretical PMS evolutionary tracks at low masses run almost vertically in the H-R diagramme, hence the determination of effective temperature is critical for the mass estimation of young low-mass stars. Moreover, as also seen here, among the various models there exist large differences in the predicted paths of young stars towards the main sequence, consequently the inferred masses and ages are sensitive to both the choice of models and the adopted temperature scale. In the case of the eclipsing components of RX J0529.4+0041 A, the surface gravities, calculated directly from the masses and radii, allow to restrict the choice to the temperature scales for dwarf stars.

Due to the relatively large temperature difference between the components of RX J0529.4+0041 A, the secondary eclipse appears too shallow and poorly defined, when observed in visible bands, to provide a satisfactory determination of the effective temperature of the cooler component. The situation was made even worse by the "veiling" produced on the light-curve by the third-light contribution, due to the close visual companion, unresolved in most of the optical observations. Hence, the idea to observe in the near-IR, where the secondary minimum was expected to be deeper, and to exploit adaptive optics capabilities in order to separate the light from the companion and to obtain high precision, high time-resolution, near-infrared differential light-curves.

It is also important to note that the two components of RX J0529.4+0041 A are in a well-detached binary configuration, as each star is well inside its critical Roche lobe. Thus, the current observable properties of the two stars are not expected to differ significantly from those of single stars of the same masses and age, although they will certainly become affected by binarity at some point in their future evolution, after the primary will have left the main sequence. On the other hand, it is very likely that their orbits had already experienced an early dynamical evolution, during the formation phase, which eventually led to circularization accompanied by a shrinkage of the orbit to its present-day size. Theory predicts that tidal friction in a hierarchical triple, provided that the outer and inner orbits are nearly orthogonal, can reduce the inner orbital period from months to days within a relatively short period of time, of the order of $P_{\rm out}^2/P_{\rm in}$ (Kiseleva et al. 1998). We can obtain a rough evaluation (or at least the order of magnitude) for the orbital period of the outer binary from the third Kepler law, by adopting a total mass $M_{\rm tot} = 3\ M_\odot$ (with $M_{\rm A} = 2.2\ M_\odot$ and assuming $M_{\rm B} = 0.8\ M_\odot$), provided that the projected separation of 1.3 arcsec is not very different from the true angular semi-major axis of the orbit (following the statistical arguments by Reipurth & Zinnecker 1993). Then, at a distance of 325 pc, this translates into a semi-major axis $a \approx 400$ AU, or an orbital period of $P_{\rm out} \approx 1.4 \times 10^4$ yr. Thus, a rough upper limit to the time required to reduce the orbital period of the inner binary from a few months to the present value of 3 days (with a parallel increase of the outer orbit period) would be of the order of 10^8 years. This means that such a mechanism could plausibly operate to determine the present-day orbital configuration of the RX J0529.4+0041 triple system.

We notice that, in the case of synchronous rotation, the radii of the two components yield equatorial rotational velocities of 24.4 and 23 km s^{-1} for the Primary and Secondary components, respectively. The result is thus fully consistent with the measured $v \sin i$ of 25 ± 3 km s^{-1} for the Primary, while it appears somewhat in excess with respect to the value of 17 ± 3 km s^{-1} measured in the case of the Secondary, unless the accuracy of the $v \sin i$ measurement is notably worse than the quoted statistical error. Thus, this might indicate that either the radius of the Secondary is significantly overestimated (by about 20%), or the synchronization condition is not verified for the lower-mass

component. However, the latter eventuality appears less likely, because spin-orbit synchronization is expected to occur on a shorter time-scale than orbital circularization (Zahn & Bouchet 1989).

The new observations presented here have shown that it is indeed possible to improve significantly the visibility and the definition of the secondary eclipse, and, in principle, the overall quality of the entire light-curve by means of spatially resolved near-IR photometry. However, due to the severe constraints set by the three-day orbital period, the main limitation of ground-based observations is the difficulty in covering the full light-curve by observing over a few, consecutive, orbital cycles. This makes any attempt towards a more detailed analysis of the light-curve and the interpretation of possible out-of-eclipse variations in terms of the presence of stellar spots far more complicated. Indeed, although the wavy shape of the light-curves outside eclipse clearly indicates the presence of spots on at least one of the components, the present data-set appears inadequate for a meaningful, detailed treatment of stellar spots (Torres & Ribas 2002).

Therefore, the best way to carry out a fine light-curve analysis and further improve the present determinations of the stellar parameters for RX J0529.4+0041 A, and possibly for other PMS eclipsing systems, would be to ensure continuous phase coverage observations, over at least two consecutive orbital cycles, exploiting for instance photometric telescopes on board satellites.

Acknowledgements. We wish to thank the ESO staff for kind assistance and technical support during the ADONIS observations, in particular Katie Brooks and Erich Wenderoth. We also gratefully acknowledge Antonio Magazzù and Javier A. Licandro for performing the service observations at the TNG. We thank the referee, Dr. J. Andersen, for valuable comments which helped to improve the paper. We acknowledge financial support by the Italian *Ministero dell'Università e della Ricerca*. This research has made use of the Simbad database, operated at CDS, Strasbourg, France.

References

Alcalá, J. M., Covino, E., Melo, C., & Sterzik, M. F. 2002, A&A, 384, 521
Alencar, S. H. P., & Vaz, L. P. R. 1997, A&A, 326, 257
Alonso, A., Arribas, S., & Martínez-Roger, C. 1996, A&A, 313, 873
Amado, P. J., & Byrne, P. B. 1997, A&A, 319, 967
Andersen, J. 1991, A&AR, 3, 91
Baraffe, I., Chabrier, G., Allard, F., & Hauschildt, P. H. 1998, A&A, 337, 403
Baraffe, I., Chabrier, G., Allard, F., & Hauschildt, P. H. 2002, A&A, 382, 563
Barnes, T. G., Evans, D. S., & Moffett, T. J. 1978, MNRAS, 183, 285
Beuzit, J.-L., Demailly, L., Gendron, E., et al. 1997, Exper. Astron., 7, 285
Covino, E., Catalano, S., Frasca, A., et al. 2000, A&A, 361, L49
Covino, E., Melo, C. H. F., Alcalá, J. M., et al. 2001, A&A, 375, 130
Cox, A. N. 2000, Allen's Astrophysical Quantities, 4th ed. (New York: AIP Press and Springer-Verlag)
D'Antona, F., & Mazzitelli, I. 1997, in Proc. of Cool stars in clusters and associations: Magnetic activity and age indicators Mem. S.A.It., ed. G. Micela, R. Pallavicini, & S. Sciortino, 68, 807
D'Antona, F., Ventura, P., & Mazzitelli, I. 2000, ApJ, 543, L77
de Jager, C., & Nieuwenhuijzen, H. 1987, A&A, 177, 217
Devillard, N. 1997, The Messenger, 87, 19
Djurašević, G. 1992, Ap&SS, 196, 241
Flower, P. J. 1996, ApJ, 469, 355
Gray, D. F. 1992, The observation and analysis of stellar photospheres, Cambridge Astrophysics Ser. (Cambridge University Press)
Hauschildt, P. H., Allard, F., & Baron, E. 1999a, ApJ, 512, 377
Hauschildt, P. H., Allard, F., Ferguson, J., Baron, E., & Alexander, D. R. 1999b, ApJ, 525, 871
Hendry, P. D., & Mochnacki, S. W. 1992, ApJ, 388, 603
Hofmann, R., Brandl, B., Eckart, A., Eisenhauer, F., & Tacconi-Garman, L. 1995, High angular-resolution NIR astronomy with large arrays (SHARP I and SHARP II), SPIE, 2475, 192
Houdashelt, M. L., Bell, R. A., & Sweigart, A. V. 2000, AJ, 119, 1448
Hunt, L. K., Mannucci, F., & Testi, L., et al. 1998, AJ, 115, 2594
Kiseleva, L. G., Eggleton, P. P., & Mikkola, S. 1998, MNRAS, 300, 292
Lamla, E. 1982, in Landolt-Bornstein Ser., Vol 2b Stars and Star Clusters, ed. K. Schaifers, & H. H. Voight (Berlin: Springer-Verlag)
Lee, C. W., Martin, E. L., & Mathieu, R. D. 1994, AJ, 108, 1445
Mathieu, R. D. 1994, ARAA, 32, 465
Melo, C. H. F., Covino, E., Alcalá, J. M., & Torres, G. 2001, A&A, 378, 898
Palla, F., & Stahler, S. W. 1999, ApJ, 525, 772
Reipurth, B., & Zinnecker, H. 1993, A&A, 278, 81
Rucinski, S. M. 1969, Acta Astron., 19, 245
Savage, B. D., & Mathis, J. S. 1979, ARA&A, 17, 73
Simon, M., Dutrey, A., & Guilloteau, S. 2000, ApJ, 545, 1034
Stahler, S. W. 1988, ApJ, 332, 804
Stassun, K. G., Mathieu, R. D., Vaz, L. P. Stroud, N., & Vrba, F. 2004, ApJS, 151, 357
Steffen, A., Mathieu, R. D., Lattanzi, M. G., et al. 2001, AJ, 122, 997
Swenson, F. J., Faulkenr, J., Rogers, F. J., & Iglesias, C. A. 1994, ApJ, 425, 286
Torres, G., & Ribas, I. 2002, ApJ, 567, 1140
Van Hamme, W. 1993, AJ, 106, 2096
Zahn, J.-P., & Bouchet, L. 1989, A&A, 223, 112
Wichmann, R., Covino, E., Alcalá, J. M., et al. 1999, MNRAS, 307, 909
Wilson, R. E. 1994, PASP, 106, 921

Online Material

Appendix A: Third-light correction

The net effect of the presence of a third light on the light-curve is to produce a kind of veiling, which reduces the depths of the eclipses as well as their ratio, thus simulating a system with lower orbital inclination and altered temperature difference between the eclipsing components.

The total flux contributed by the two eclipsing components (indicated by the indices 1 and 2) at phase ϕ is

$$l(\phi) = l_1(\phi) + l_2(\phi).$$

Let us denote with $l^\star$ the total flux contributed by the eclipsing components at maximum light (i.e, corresponding to the out-of-eclipse level), and with l_3 the flux from the third light, that we assume to be constant. Correspondingly, the combined flux, including the constant contribution from the third light, is

$$l_{\rm comb}(\phi) = l(\phi) + l_3$$

and, at maximum light,

$$l^\star_{\rm comb} = l^\star + l_3$$

Hence, the combined magnitudes at phase ϕ and maximum light, respectively, will be:

$$m_{\rm comb} = -2.5 \log(l(\phi) + l_3) + c \quad \text{(A.1)}$$

$$m^\star_{\rm comb} = -2.5 \log(l^\star + l_3) + c \quad \text{(A.2)}$$

c being a constant, and the magnitude variation with respect to maximum light is:

$$\Delta m_{\rm comb} = m_{\rm comb} - m^\star_{\rm comb} = -2.5 \log\left(\frac{l(\phi) + l_3}{l^\star + l_3}\right)$$

$$= -2.5 \log\left(\frac{l(\phi)/l^\star + \gamma}{1 + \gamma}\right) \quad \text{(A.3)}$$

Table 1. *JHK* differential photometry of the eclipsing component RXJ 0529.4+0041 A with respect to component B, with running Heliocentric Julian Day (-2,400,000). The corresponding orbital phase is computed using the new ephemeris given in Sec. 4.1 **(Only in electronic form.)**

HJD	Phase	ΔJ
51886.55859	0.95086	-0.980
51886.56250	0.95215	-0.958
51886.57031	0.95472	-0.975
51886.59766	0.96372	-0.931
51886.60547	0.96629	-0.897
51886.61328	0.96887	-0.911
51886.61719	0.97015	-0.909
51886.62500	0.97272	-0.898
51886.62891	0.97401	-0.867
51886.63281	0.97530	-0.835
51886.63672	0.97658	-0.791
51886.64453	0.97915	-0.770
51886.64844	0.98044	-0.741
51886.65234	0.98173	-0.700
51886.66016	0.98430	-0.659
51886.66406	0.98558	-0.622
51886.66797	0.98687	-0.578
51886.67578	0.98944	-0.530
51886.67969	0.99073	-0.493
51886.68359	0.99201	-0.455
51886.68750	0.99330	-0.417
51886.69531	0.99587	-0.395
51886.69922	0.99716	-0.376
51886.70312	0.99844	-0.372
51886.71094	0.00101	-0.372
51886.71484	0.00230	-0.390
51886.71875	0.00359	-0.410
51886.72656	0.00616	-0.441
51886.73047	0.00744	-0.476
51886.73438	0.00873	-0.519
51886.73828	0.01002	-0.559
51886.74609	0.01259	-0.598
51886.75000	0.01387	-0.634
51886.75391	0.01516	-0.670
51886.76172	0.01773	-0.732
51886.76953	0.02030	-0.762
51886.77344	0.02159	-0.782
51886.77734	0.02288	-0.812
51886.78125	0.02416	-0.846
51886.78906	0.02673	-0.872
51886.79297	0.02802	-0.910
51886.79688	0.02931	-0.922
51886.80469	0.03188	-0.944
51886.80859	0.03316	-0.951
51886.81250	0.03445	-0.962
51886.81641	0.03573	-0.966
51886.82422	0.03831	-0.983
51886.82812	0.03959	-0.984
51886.83594	0.04216	-0.980
51921.55078	0.47025	-0.998
51921.55859	0.47282	-0.981
51921.56641	0.47539	-0.949
51921.57422	0.47796	-0.933
51921.57812	0.47925	-0.917
51921.58203	0.48053	-0.890
51921.58984	0.48311	-0.871
51921.59375	0.48439	-0.853
51921.59766	0.48568	-0.829
51921.60547	0.48825	-0.808
51921.60938	0.48954	-0.789
51921.61719	0.49211	-0.769
51921.62109	0.49339	-0.750

where $\gamma = l_3/l^\star$. From this,

$$\frac{l(\phi)}{l^\star} = 10^{-0.4\Delta m_{\rm comb}}(1+\gamma) - \gamma. \quad \text{(A.4)}$$

The latter equation can be expressed as differential corrected magnitude

$$\Delta m_{\rm corr} = -2.5 \log \frac{l(\phi)}{l^\star} =$$

$$= -2.5 \log[10^{-0.4\Delta m_{\rm comb}}(1+\gamma) - \gamma] \quad \text{(A.5)}$$

where the only unknown quantity is γ. This latter can be derived if it is possible to resolve and measure separately the visual components (as we did on ADONIS images and on a few OIG images). In order to determine γ, it is sufficient to know the magnitude difference between the visual components at maximum light, which is:

$$\Delta m^\star = -2.5 \log \frac{l^\star}{l_3} = +2.5 \log \gamma \quad \text{(A.6)}$$

and, from this, one obtains:

$$\gamma = 10^{0.4\Delta m^\star}. \quad \text{(A.7)}$$